Flexoelectric Effect in the Reversal of Self-Polarization and Associated Changes in the Electronic Functional Properties of $BiFeO_3$ Thin Films

Byung Chul Jeon, Daesu Lee, Myang Hwan Lee, Sang Mo Yang, Seung Chul Chae, Tae Kwon Song, Sang Don Bu, Jin-Seok Chung, Jong-Gul Yoon, and Tae Won Noh*

Flexoelectricity is the generation of an electric field by a strain gradient via electro-mechanical coupling. This effect was predicted theoretically by Kogan in 1964[1] and experimentally observed by Bursian and Zaikovskii in 1968.[2] The phenomenon was given the name 'flexoelectricity' by Indenbom et al. in 1981.[3] Despite its long history, there has been little research on flexoelectricity of bulk solid materials,[3–13] because its effects had been widely accepted to be quite small. Namely, the flexoelectric coefficients are small (10^{-10}–10^{-11} C m^{-1}),[12] and the strain gradients generated by mechanical bending are quite small, typically on the order of 0.1 m^{-1}.[13]

Recently, there has been much interest in flexoelectricity, especially regarding epitaxial thin films.[14–20] Inside these material systems, a strain gradient as large as 10^5–10^6 m^{-1} can be produced.[14,15] Note that this value of the strain gradient is 6 or 7 orders of magnitude larger than the corresponding bulk values. Using numerous epitaxial ferroelectric thin films, experimental studies showed that flexoelectricity can affect the domain configuration and imprint,[15] dielectric constant,[16,17] continuous rotation of the spontaneous polarization direction,[18] polarization switching by mechanical force,[19] and unusual coupling between electronic transport and the mechanical strain gradient.[20]

Prof. S. D. Bu
Department of Physics
Chonbuk National University
Jeonju, 561–756, Korea
E-mail: sbu@chonbuk.ac.kr
B. C. Jeon, Dr. D. Lee, Dr. S. M. Yang, Dr. S. C. Chae, Prof. T. W. Noh
Center for Functional Interfaces of Correlated Electron Systems
Institute for Basic Science (IBS)
Seoul, 151–747, Korea
Department of Physics and Astronomy
Seoul National University
Seoul, 151–747, Korea
M. H. Lee, Prof. T. K. Song
School of Nano and Advanced Materials Engineering
Changwon National University
Changwon, 641–773, Korea
Prof. J.-S. Chung
Department of Physics
Soongsil University
Seoul, 156–743, Korea
Prof. J.-G. Yoon
Department of Physics
University of Suwon
Hwaseong, 445–743, Korea

DOI: 10.1002/adma.201301601

Many ferroelectric films were reported to have one preferred polarization direction just after deposition.[21–29] This phenomenon, known as a self-polarization, has been attributed to a built-in electric field.[21–30] Numerous origins have been proposed for the built-in electric field, namely defects,[21] piezoelectricity,[24] interfacial electrode effects,[25–29] and so on. Specifically for $BiFeO_3$ (BFO) thin films, most of the earlier research showed that the as-grown films usually exhibited downward self-polarization.[25–28] Here, we show how flexoelectricity can reverse the direction of the as-grown polarization in epitaxial BFO thin films grown on a vicinal $SrTiO_3$ (STO) substrate with an $SrRuO_3$ (SRO) bottom electrode. In addition, the change in the self-polarization could result in large variations of the functional properties of the as-grown BFO films, including ferroelectric hysteresis and diode behavior.

Figure 1a shows the X-ray diffraction (XRD) θ–2θ scan for 250 nm thick BFO films grown at 570 and 550 °C. For these films, only the BFO (00*l*) peaks appear, indicating that the crystalline axes of the films were well-aligned. The BFO (002) peaks for both the films were located between the predicted positions for the fully strained BFO film and bulk BFO, shown as the dotted and solid lines, respectively. This indicated that some structural relaxation occurred for both the films. In addition, the BFO (002) peak position of the film grown at 550 °C was closer to the bulk BFO value, indicating that this film became more relaxed along the [001] direction than that grown at 570 °C.

Although deposition temperature (T_D) differed by only 20 °C, we found that our BFO thin films had different strain relaxation behaviors. To obtain information on the in-plane strain state, we used reciprocal space mapping (RSM) analysis of the {103} family of BFO peaks with various ϕ angles for the 250 nm thick BFO films (Figure 1b,c).[28] The (013) and ($0\,\bar{1}\,3$) BFO Bragg peaks for the film grown at 570 °C are located near the vertically dotted line, indicating that this film was almost fully strained along the [010] direction, while the ($\bar{1}03$) and (103) BFO Bragg peaks were located outside of the vertically dotted line (Figure S1a–c, Supporting Information), indicating that this film was relaxed along the [100] direction. From here on, the films grown at 570 °C will be referred to as uniaxially strained BFO (US-BFO) films. Figures 1c and S1d–f show the RSM results for the film grown at 550 °C. Note that the {103} family of peaks are located outside of the vertically dotted line, indicating that the film was relaxed in all directions; these films will be referred to as relaxed BFO (R-BFO) films.

To obtain further information on how strain developed in the US-BFO films, we deposited four BFO films at 570 °C with

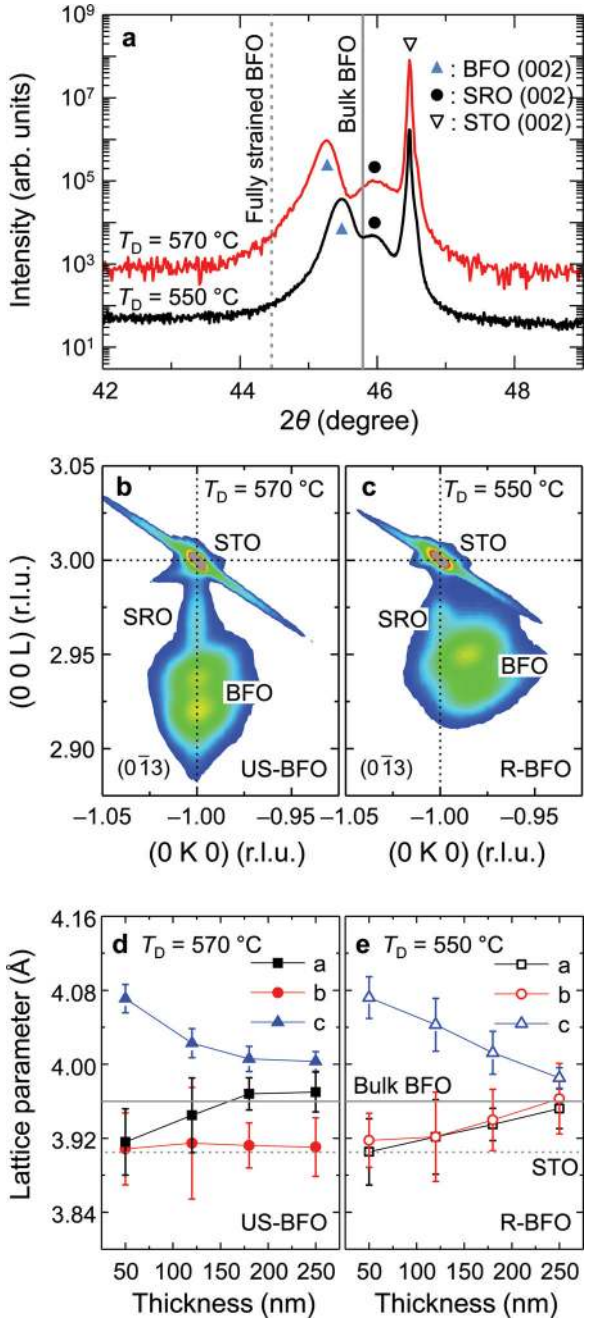

Figure 1. a) XRD θ–2θ scans of the 250 nm thick BFO films grown at 570 (solid red line) and 550 °C (solid black line) on vicinal STO (001) substrates. The gray short-dashed and solid vertical lines indicate the (002) diffraction peak positions of the fully strained and relaxed BFO films on STO substrates, respectively. b,c) RSM images around the (0$\bar{1}$3) STO Bragg peaks for US- and R-BFO films, respectively. d,e) Pseudocubic lattice parameters as a function of the film thickness for US- and R-BFO films, respectively. The solid and dotted gray lines represent the lattice parameter of bulk BFO and STO, respectively.

four different thicknesses of 50, 120, 180, and 250 nm. (Their XRD θ–2θ and RMS data are shown in Figure S2, Supporting Information.) The 50 nm thick film is fully strained in the *ab*-plane. As the film thickness increased, the average value of the *c*-axis lattice constant decreased, but the *b*-axis lattice constant remained constant (Figure S2, Supporting Information). We determined the average values of all the lattice constants from the θ–2θ and RSM data. The results are shown in Figure 1d. Note that the average value of the *b*-axis lattice constant was independent of the film thickness and nearly the same as that of the STO substrate. Because the *b*-axis corresponds to the direction of step edges in STO substrates, the uniaxially strained growth behaviors should originate from clamping effects of the US-BFO films at the STO step edges.

Based on the structural data, we proposed a schematic diagram of the US-BFO films (Figure S3, Supporting Information). According to our RSM analysis, the US-BFO films were strongly clamped along the [010] direction. Along that direction, the lattice constant of the in-plane BFO near the substrate might be the same as that of the substrate. Experimentally, we found that this as-grown film should have a downward polarization. With the preferential distortion of the BFO unit cells on the miscut STO substrate, only two polarization variants, P_1^- and P_4^-, are possible.[27]

To obtain information on the strain evolution of R-BFO films, we also deposited four BFO films at 550 °C with thicknesses of 50, 120, 180, and 250 nm. (Their XRD θ–2θ and RMS data are shown in Figure S4, Supporting Information.) Similar to the US-BFO case, this 50 nm thick film was fully strained in the *ab*-plane. However, above a critical thickness, all of the thicker films became relaxed along the *b*-axis as well as along the *a*-axis, contrary to the US-BFO films. Figure 1e shows the average values of their lattice constants, evaluated from XRD data. These data showed that the strain relaxation occurred progressively in all directions. Although T_D was lower by only 20 °C, compared with that of the US-BFO films, the step edges of the STO substrate could not clamp the BFO layer effectively in the R-BFO films.

Figure 2 shows our proposed schematic diagram of the strain states of R-BFO films. Near the substrate, the BFO layers were fully strained. However, above the critical thickness, strain relaxation should occur in all directions. It should be noted that the *b*-axis lattice near the step edge could be somewhat more strained than those far from the step edge due to the clamping effect, as shown in Figure 2a. As a result, there should be an expansion of the *b*-axis lattice constant along the [100] direction. This strain gradient, $\partial u_{22}/\partial x_1$, will generate a horizontal electric field by flexoelectricity (large red arrow in Figure 2a). Note that u_{jk} and x_i are the strain and spatial coordinates of the film (*i*, *j*, and *k* = 1, 2, and 3).[4,7] In addition, there should be vertical electric fields due to $\partial u_{11}/\partial x_3$, $\partial u_{22}/\partial x_3$, and $\partial u_{33}/\partial x_3$ (large blue arrow in Figure 2c), which come from the relaxation of the *a*-, *b*-, and *c*-axis lattice constants along the [001] direction. Note that the $\partial u_{22}/\partial x_1$ and $\partial u_{22}/\partial x_3$ terms can appear only for the R-BFO films. We argue that these new strain gradient terms could reverse the downward self-polarization direction of R-BFO films to an upward self-polarization.

To measure the self-polarization direction, we performed piezoresponse force microscopy (PFM) experiments. The as-grown BFO films deposited at 570 °C always had downward self-polarization, irrespective of whether they were fully or uniaxially strained (**Figure 3**a). In contrast, the film deposited at 550 °C with a thickness of 50 nm was fully strained and had downward self-polarization (the first picture of Figure 3b). However,

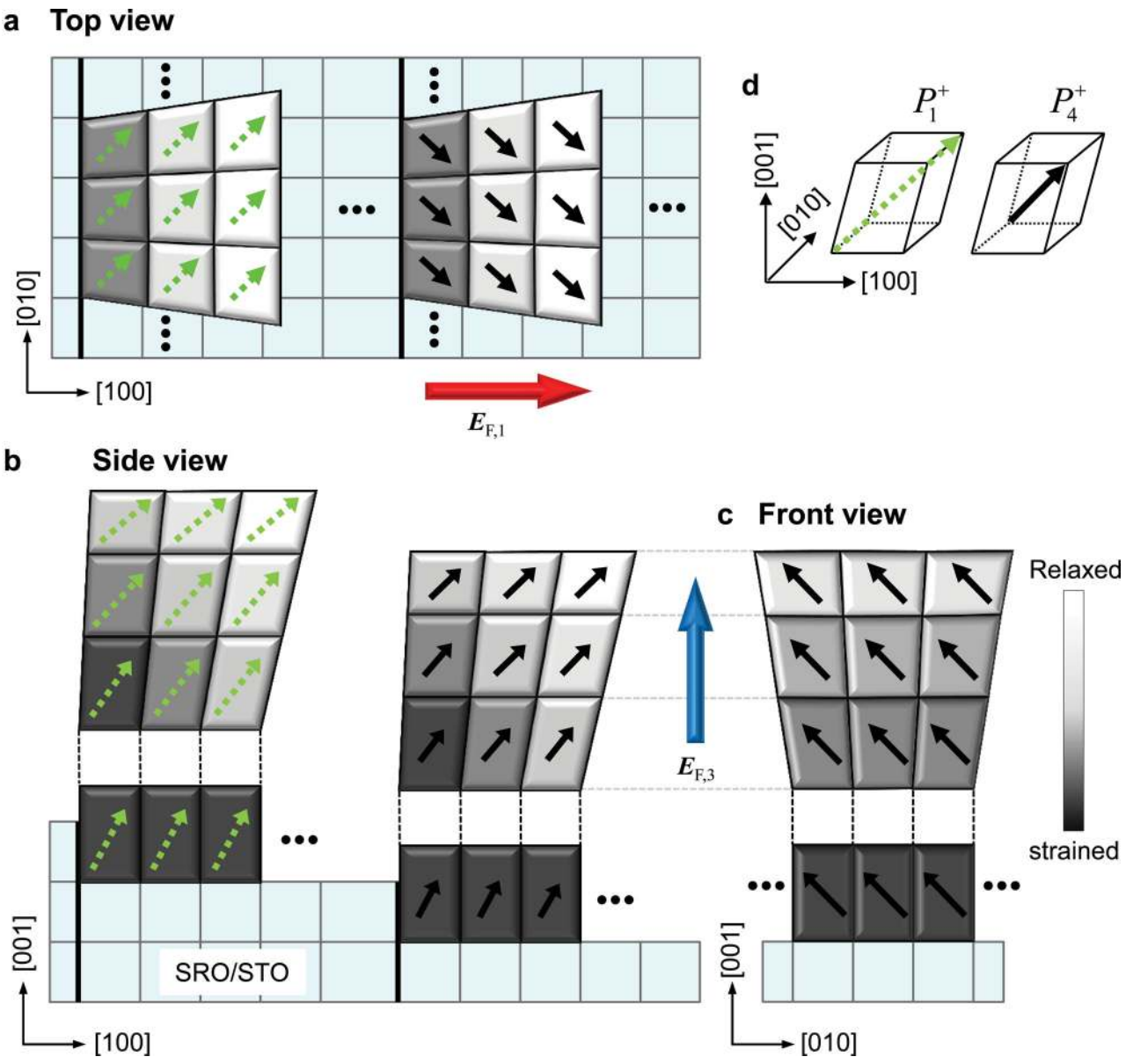

Figure 2. Schematic diagram of the direction of the strain relaxation for R-BFO films. The dark and pale gray areas represent strongly strained and relaxed regions, respectively. a–c) Schematic diagram top, side, and front views, respectively. The large red and blue arrows indicate the direction of the horizontal ($E_{F,1}$) and vertical ($E_{F,3}$) flexoelectric fields, respectively. d) Possible polarization orientation for R-BFO films. The green-dotted and black solid-line arrows indicate the direction of ferroelectric polarization, P_1^+ and P_4^+, respectively. The step-bunching process and lattice dislocations (higher-order terms) are neglected in this representation (Figure S3, Supporting Information).[31]

as the film thickness increased the self-polarization direction changed from down to up (Figure 3b). These results indicate that the polarization direction of the as-grown films is not determined by particular defects, but depends on the film thickness and strain relaxation. Note that the structural change from fully strained to the relaxed state also occurred for thicknesses in the range of 50 to 120 nm, as shown in Figures 1d and 1e. Namely, the change in the self-polarization direction seems to be closely related to a change of the strain state for R-BFO films. Moreover, we measured polarization–voltage (*P*–*V*) hysteresis loops and found that the imprints of the R-BFO films with a thickness larger than 100 nm were opposite to those of the US-BFO films, consistent with changes in the self-polarization direction (for details, see Supporting Information).

To explain the reversal of the self-polarization mechanism, we suggested a schematic diagram, as shown in Figure 3c. Recently, Yu et al. demonstrated that the self-polarization direction could be engineered by varying the termination layer of the bottom electrode.[22] Balke et al. reported that the self-polarization direction is determined by the internal field produced by the different interface charges.[29] Note that both the fully strained and US-BFO films always had downward self-polarization because of the dominant interfacial electrode effect, in agreement with earlier reports.[25–28] However, for our R-BFO films, we propose

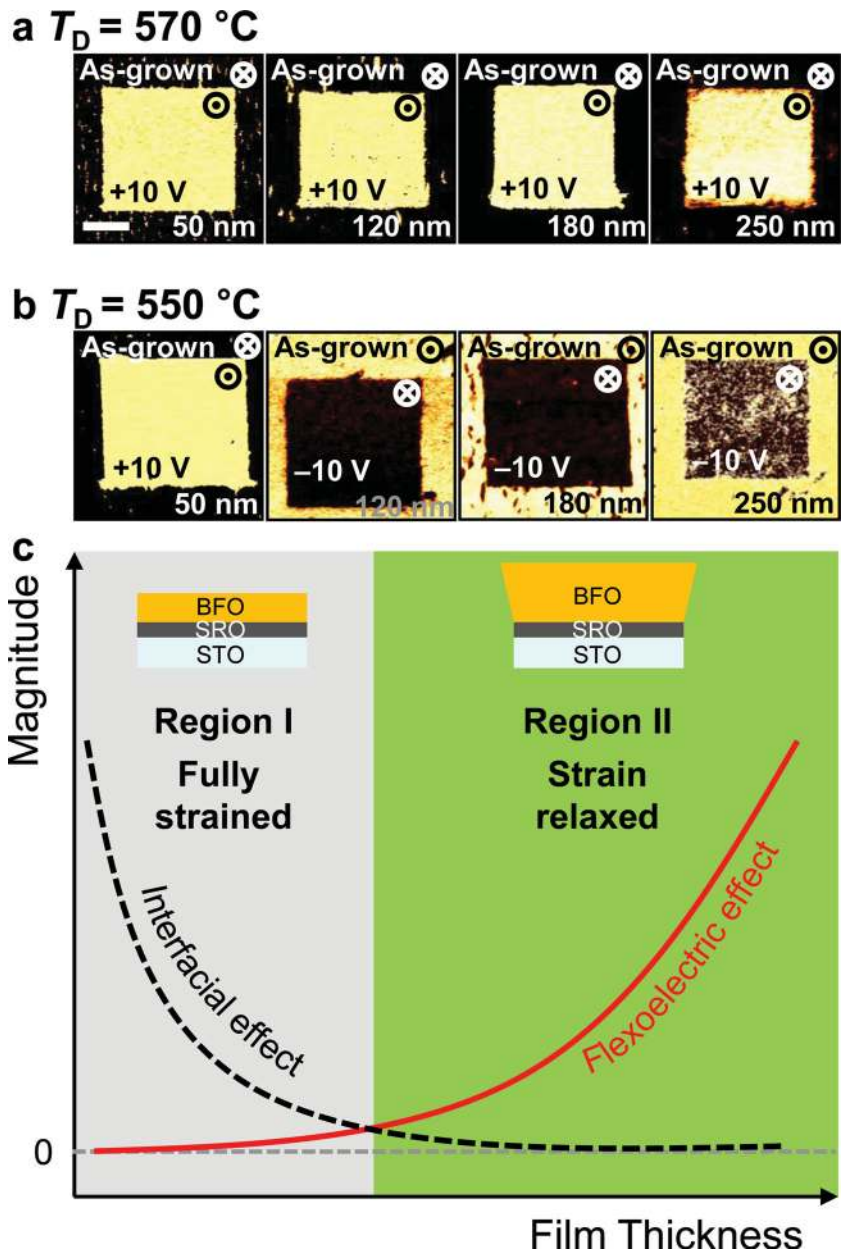

Figure 3. a,b) Out-of-plane PFM images with 50, 120, 180, and 250 nm thick BFO films. The bright yellow and dark regions indicate the up- and down-polarization states, respectively. c) Magnitude of the flexoelectric and interfacial effects as a function of film thickness. The red and black-dashed curves indicate the flexoelectric and interfacial effects, respectively. The right and left insets indicate the fully strained and relaxed BFO films, respectively.

that the above-mentioned additional strain gradient terms, i.e., $\partial u_{22}/\partial x_1$ and $\partial u_{22}/\partial x_3$, can generate the electric fields by flexoelectricity. With an increase in the film thickness, this flexoelectric effect should compete with the interfacial effects.

To obtain more quantitative information, we estimated the values of the out-of-plane and in-plane strain gradients using a Williamson–Hall (W-H) plot.[17,32] The W-H plots of BFO films were obtained from the XRD θ–2θ and RSM peak widths,[32] as shown in Figure S6 (for details, see Supporting Information). We estimated the out-of-plane strain gradient along [001], which correspond to $\partial u_{33}/\partial x_3$, as -0.5×10^5 m^{-1} and -0.7×10^5 m^{-1} for the US- and R-BFO films, respectively. We also estimated the in-plane strain gradients to be 0.2×10^5 m^{-1} and 1.9×10^5 m^{-1} for the US- and R-BFO films, respectively.

With the experimentally obtained values of strain gradient, we could estimate the flexoelectric fields, $E_{F,i}$ (i = 1, 2, and 3), using:[19,20]

$$E_{F,i} \approx \lambda \frac{e}{\varepsilon_0 a_j} \frac{\partial u_{jk}}{\partial x_i} \quad (1)$$

where λ is a scaling factor, e is the electronic charge, a_j is the lattice constant, and ε_0 is the permittivity of free space. Usually, in perovskite oxide systems, λ is known to have a value on the order of 10^0 or 10^1 (e.g., λ = 0.725 and 14.5 for $PbMg_{1/3}Nb_{2/3}O_3$ and $Ba0_{.67}Sr_{0.33}TiO_3$, respectively).[33] To the best of our knowledge, the precise value of λ is not known yet for BFO. By assuming λ = 1, we estimated $E_{F,1}$ for R-BFO to be ≈8.7 MV m^{-1}, while $E_{F,1}$ for US-BFO was estimated to be one order of magnitude weaker than that of the R-BFO. Similarly, we could estimate the vertical magnitude of the flexoelectric field, $E_{F,3}$ to be 2.3 and 3.2 MV m^{-1} for US-BFO and R-BFO, respectively. The ferroelectric polarization in BFO is [111]-oriented; thus, the effect of both the vertical and horizontal components of the flexoelectric field should be considered with regard to polarization reversal. As a result, the flexoelectric field in R-BFO is much higher, compared with that of the US-BFO film. In addition, the estimated magnitude of the flexoelectric field in R-BFO gradually became comparable to that of the coercive field for BFO at high temperatures during the growth.[33] Therefore, the flexoelectric effect should play an important role in reversing the self-polarization direction in R-BFO films.

It is well known that the configuration of defects, such as oxygen vacancies, V_O, in ferroelectric films can be determined by the polarization state, especially at high growth temperatures.[34–36] Because BFO has a very high Curie temperature of 830 °C, our BFO films should be in a ferroelectric state during the growth process. Thus, the generated self-polarization will drive V_O to one of the interfacial regions to compensate for the negative polarization charge during the growth.[34] For US- and R-BFO films, an interfacial V_O-rich defect layer formed at the top and bottom interfaces, respectively, as shown in **Figure 4**a and 4d. In addition, to satisfy the lowest energy configuration in the ferroelectric material, the defect dipoles (D_{defect}) should be aligned along the spontaneous polarization direction during the growth, resulting in imprint.[35,36] The different locations of the V_O-rich defect layer and alignment of D_{defect} can result in changes of diode characteristics and ferroelectric hysteresis, respectively.

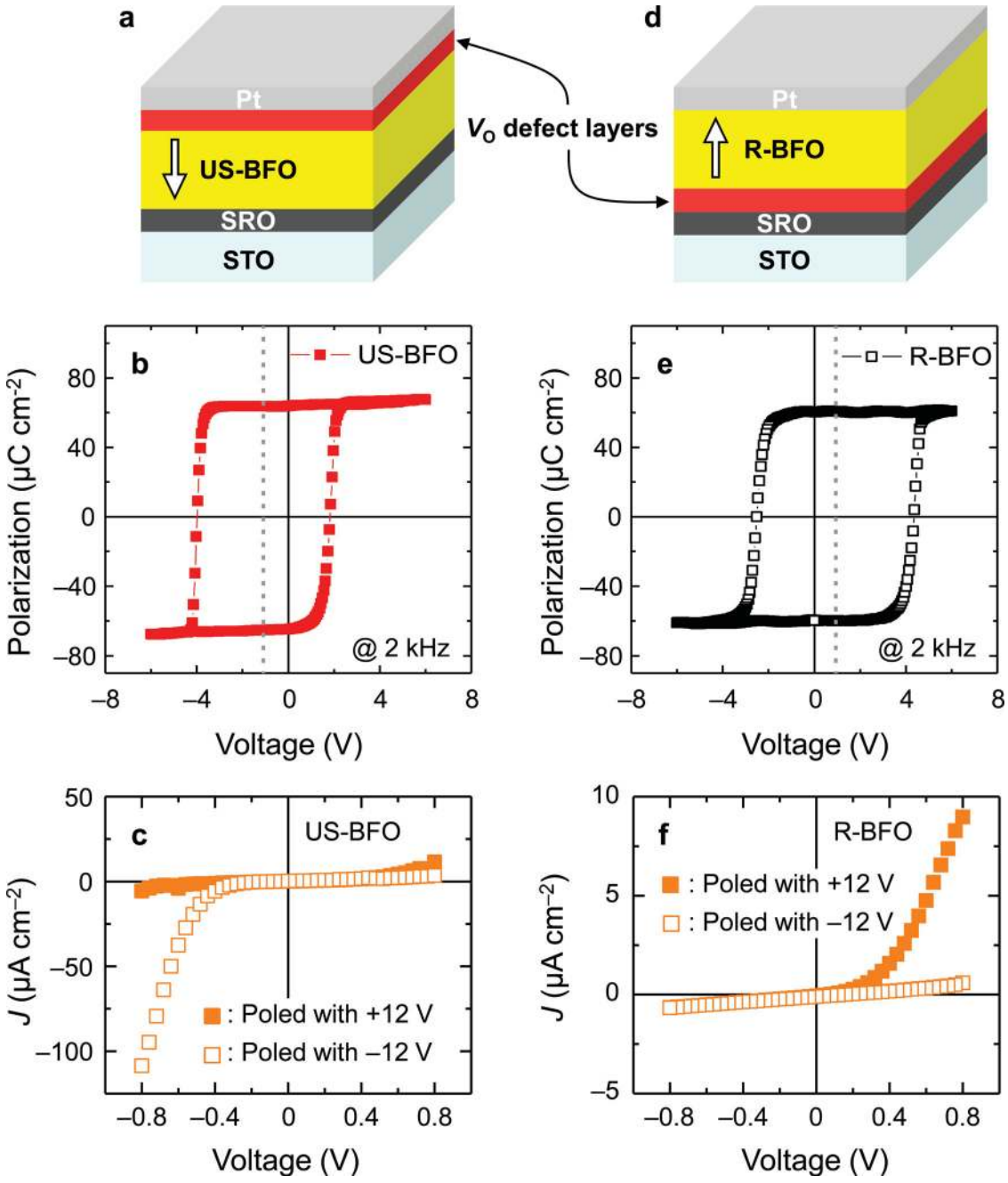

Figure 4. a,d) Schematic diagram of the location of the V_O-rich defect layer in US- and R-BFO films, respectively. The large white arrows represent the as-grown polarization direction. b,e) *P*–*V* hysteresis loops of the US- and R-BFO films, respectively. Vertical gray-dashed lines indicate the voltage center of hysteresis loops. c,f) *J*–*V* curves of US- and R-BFO films, respectively.

To confirm the configuration of the D_{defect} alignment to the imprint, we measured the *P*–*V* hysteresis loops for 250 nm thick US- and R-BFO films, as shown in Figure 4b and 4e. The remnant polarization values along the [001] pseudocubic direction were nearly the same, i.e., approximately 65 and 60 μC cm^{-2}, respectively.[25,27] Figure 4b shows a US-BFO film with a negative imprint; namely, its coercive voltages are +1.9 V for a positive bias and –4.0 V for a negative bias. In contrast, the R-BFO film shows a positive imprint; namely, its coercive voltages are +4.4 V for a positive bias and –2.5 V for a negative bias. The two BFO films exhibited different imprint characteristics, as expected.

In addition, it is already known that the defect layers at the interface can affect the transport properties such as diode behavior.[34] We measured the current density–voltage (*J*–*V*) curves for 250 nm thick US- and R-BFO films. Figure 4c shows that the *J*–*V* curves for the US-BFO film measured between –0.8 and +0.8 V, which were much smaller than the coercive

voltages.[34] The small sweep voltage range ensured that no polarization switching occurred during the measurements. In the case of an ideal BFO capacitor, the hole carriers can be injected from the electrodes when a positive bias is applied. However, if the defective layer is located at the interface, it could disturb the carrier injection process. With a negative poling (i.e., a single domain of upward polarization), the *J–V* curve exhibited reverse diode behavior. Conversely, with positive poling (i.e., a single domain of downward polarization), the *J–V* curve did not show any diode behavior for the US-BFO film. On the other hand, for the R-BFO film, the *J–V* curve should exhibit forward diode behavior with a positive poling. Conversely, with negative poling, the *J–V* curve did not show any diode behavior. Such *J–V* curves were actually observed, as shown in Figure 4f.

In summary, we found that the flexoelectric effects can play an important role in determining the self-polarization direction in the BFO thin films. We could successfully control the strain evolution of the films by varying the deposition temperature and the film thickness. Due to flexoelectric effects, the different strain gradient states inside the BFO films could then create different built-in electric fields, which resulted in changes in the self-polarization direction. In addition, the self-polarization field could also produce large variations in the imprint and diode characteristics of the as-grown BFO films by generating a defect layer and aligning the defect dipoles during the film deposition process. Thus, strain gradient engineering at the nanoscale can potentially provide exciting new opportunities to realize flexoelectricity-based devices.

Experimental Section

Thin Film Fabrication: High-quality $BiFeO_3$ (BFO) epitaxial thin films with thicknesses varying from 50 to 250 nm were fabricated. The films were sandwiched between Pt top and $SrRuO_3$ (SRO) bottom electrodes. BFO/SRO thin-film layers were fabricated using pulsed laser deposition onto $SrTiO_3$ (001) substrates with a 4° miscut toward the [100] direction. A stoichiometric BFO ceramic target was used. The BFO thin films were grown at two temperatures, i.e., 550 and 570 °C. RBS measurements showed that the films grown at 550 °C had the correct Bi and Fe stoichiometry; however, the films grown at 570 °C had a Bi/Fe ratio of about 0.95. These values, close to 1.0, suggested that our films were of high quality. On top of the BFO layer, we deposited a 40 nm thick Pt layer at room temperature by sputtering and patterned the top electrode by photolithography.

Experimental Setup and Methods: *P–V* hysteresis loops were measured using a TF analyzer 2000 (AixACCT) at room temperature. The PFM measurements were performed using an XE-100 (Park systems) with commercially available Pt/Ir-coated Si tips (PPP-EFM, Nanosensors). For PFM imaging, an AC voltage of 1.0 V rms was applied at 17.1 kHz to the bottom electrode (i.e., sample bias). The amplitude and phase signals of the converse piezoelectric responses were measured with a lock-in amplifier (SR830, Stanford Research Systems). The crystal structures of the BFO films were analyzed using high-resolution X-ray diffraction (D8 Advanced, Bruker AXS). To evaluate the in-plane strain states, reciprocal space mapping analysis of $\{\bar{1}03\}$ family peaks with various ϕ angles (0°, 90°, 180°, and 270°) was used. The average *a*-axis lattice constant was calculated from the average value of the BFO $(\bar{1}03)$ and (103) peak. The average *b*-axis lattice constant was determined from the BFO $(0\bar{1}3)$ peak value for $\phi = 90°$. The average *c*-axis lattice constant was obtained from the θ–2θ data. Current density–voltage measurements were performed at room temperature using a low-noise probe station and a picoampere meter (Keithley 236). A +12 V (–12 V) external-poling voltage was applied to the uniaxially strained (relaxed) BFO capacitor to obtain the downward (upward) polarization state; a –12 V (+12 V) external-poling voltage resulted in upward (downward) polarization.

Supporting Information

Supporting Information is available from the Wiley Online Library or from the author.

Acknowledgements

This work was supported by the Institute for Basic Science (IBS) in Korea and the National Research Foundation of Korea (NRF) (J.-G.Y.: No. 2011–0005145, J.-S. C.: No. 2009–0077249, and S.D.B.: No. 2012R1A1A2008830) grant funded by the Korea government (MEST).

Received: April 11, 2013
Published online: July 30, 2013

[1] S. M. Kogan, *Sov. Phys. Solid State* **1964**, *5*, 2069.
[2] E. V. Bursian, O. I. Zaikovskii, *Sov. Phys. Solid State* **1968**, *10*, 1121.
[3] V. L. Indenbom, E. B. Loginov, M. A. Osipov, *Kristallografiya* **1981**, *26*, 1157.
[4] A. K. Tagantsev, *Phys. Rev. B* **1986**, *34*, 5883.
[5] W. Ma, L. E. Cross, *Appl. Phys Lett.* **2001**, *78*, 2920.
[6] R. Resta, *Phys. Rev. Lett.* **2010**, *105*, 127601.
[7] R. Maranganti, P. Sharma, *Phys. Rev. B* **2009**, *80*, 054109.
[8] A. K. Tagantsev, V. Meunier, P. Sharma, *MRS Bulletin* **2009**, *34*, 643.
[9] A. Gruverman, B. J. Rodriguez, A. I. Kingon, R. J. Nemanich, A. K. Tagantsev, J. S. Cross, M. Tsukada, *Appl. Phys. Lett.* **2003**, *83*, 728.
[10] W. Ma, L. E. Cross, *Appl. Phys. Lett.* **2005**, *86*, 072905.
[11] W. Ma, L. E. Cross, *Appl. Phys. Lett.* **2006**, *88*, 232902.
[12] L. E. Cross, *J. Mater. Sci.* **2006**, *41*, 53.
[13] P. Zubko, G. Catalan, A. Buckley, P. R. L. Welche, J. F. Scott, *Phys. Rev. Lett.* **2007**, *99*, 167601.
[14] D. Lee, T. W. Noh, *Philos. Trans. A. Math. Phys. Eng. Sci.* **2012**, *370*, 4944.
[15] D. Lee, A. Yoon, S. Y. Jang, J.-G. Yoon, J.-S. Chung, M. Kim, J. F. Scott, T. W. Noh, *Phys. Rev. Lett.* **2011**, *107*, 057602.
[16] G. Catalan, L. J. Sinnamon, J. M. Gregg, *J. Phys.: Condens. Matter* **2004**, *16*, 2253.
[17] G. Catalan, B. Noheda, J. McAneney, L. J. Sinnamon, J. M. Gregg, *Phys. Rev. B* **2005**, *72*, 020102(R).
[18] G. Catalan, A. Lubk, A. H. G. Vlooswijk, E. Snoeck, C. Magen, A. Janssens, G. Rispens, G. Rijnders, D. H. A. Blank, B. Noheda, *Nat. Mater.* **2011**, *16*, 963.
[19] H. Lu, C.-W. Bark, D. Esque de los Ojos, J. Alcala, C. B. Eom, G. Catalan, A. Gruverman, *Science* **2012**, *336*, 59.
[20] D. Lee, S. M. Yang, J.-G. Yoon, T. W. Noh, *Nano Lett.* **2012**, *12*, 6436.
[21] V. P. Afanasjev, A. A. Petrov, I. P. Pronin, E. A. Tarakanov, E. J. Kaptelov, J. Graul, *J. Phys.: Condens. Matter* **2001**, *13*, 8755.
[22] P. Yu, W. Luo, D. Yi, J. X. Zhang, M. D. Rossell, C.-H. Yang, L. You, G. Singh-Bhalla, S. Y. Yang, Q. He, Q. M. Ramasse, R. Erni, L. W. Martin, Y. H. Chu, S. T. Pantelides, S. J. Pennycook, R. Ramesh, *Proc. Natl. Acad. Sci. USA* **2012**, *109*, 9710.
[23] A. L. Kholkin, K. G. Brooks, D. V. Taylor, S. Hiboux, N. Setter, *Integrated Ferroelectrics* **1998**, *22*, 525.
[24] M. D. Glinchuk, A. N. Morozovska, *Ferroelectrics* **2005**, *317*, 125.

[25] Y. H. Chu, Q. Zhan, L. W. Martin, M. P. Cruz, P. L. Yang, G. W. Pabst, F. Zavaliche, S. Y. Yang, J. X. Zhang, L. Q. Chen, D. G. Schlom, I. N. Lin, T. B. Wu, R. Ramesh, *Adv. Mater.* **2006**, *18*, 2307.
[26] Y. H. Chu, M. P. Cruz, C. H. Yang, L. W. Martin, P. L. Yang, J. X. Zhang, K. Lee, L. Q. Chen, R. Ramesh, *Adv. Mater.* **2007**, *19*, 2662.
[27] H. W. Jang, D. Ortiz, S. H. Baek, C. M. Folkman, R. R. Das, P. Shafer, Y. Chen, C. T. Nelson, X. Pan, R. Ramesh, C. B. Eom, *Adv. Mater.* **2009**, *21*, 817.
[28] S. H. Baek, H.W. Jang, C. M. Folkman, Y. L. Li, B. Winchester, J. X. Zhang, Q. He, Y. H. Chu, C. T. Nelson, M. S. Rzchowski, X. Q. Pan, R. Ramesh, L. Q. Chen, C. B. Eom, *Nat. Mater.* **2010**, *9*, 309.
[29] N. Balke, I. Bdikin, S. V. Kalinin, A. L. Kholkin, *J. Am. Ceram. Soc.* **2009**, *92*, 1629.
[30] Z. Wang, X. X. Zhang, X. Wang, W. Yue, J. Li, J. Miao, W. Zhu, *Adv. Funct. Mater.* **2012**, *23*, 124.
[31] T. H. Kim, S. H. Baek, S. Y. Jang, S. M. Yang, S. H. Chang, T. K. Song, J.-G. Yoon, C. B. Eom, J.-S. Chung, T. W. Noh, *Appl. Phys. Lett.* **2011**, *98*, 022904.
[32] G. K. Williamson, W. H. Hall, *Acta Metall.* **1953**, *1*, 22.
[33] W. Ma, *Phys. Status Solidi B* **2008**, *245*, 761.
[34] D. Lee, S. H. Baek, T. H. Kim, J.-G. Yoon, C. M. Folkman, C. B. Eom, T. W. Noh, *Phys. Rev. B* **2011**, *84*, 125305.
[35] D. Lee, B. C. Jeon, S. H. Baek, S. M. Yang, Y. J. Shin, T. H. Kim, Y. S. Kim, J.-G. Yoon, C. B. Eom, T. W. Noh, *Adv. Mater.* **2012**, *24*, 6490.
[36] C. M. Folkman, S. H. Baek, C. T. Nelson, H. W. Jang, T. Tybell, X. Q. Pan, C. B. Eom, *Appl. Phys. Lett.* **2010**, *96*, 052903.